Research Article | Vol. 1, No. 2 | 15 Oct 2018 | OSA CONTINUUM 727
OSA CONTINUUM

Metasurfaces, dark modes, and high NA illumination

LUKAS WESEMANN,[1,*] PANJI ACHMARI,[1] KALPANA SINGH,[1] EVGENIY PANCHENKO,[1] TIMOTHY D. JAMES,[1] DANIEL E. GÓMEZ,[2] TIMOTHY J. DAVIS,[1] AND ANN ROBERTS[1]

[1]*School of Physics, The University of Melbourne, 3010, Australia*
[2]*Centre of Excellence for Exciton Science, RMIT University, GPO Box 2476, Melbourne VIC 3001, Australia*
**lwesemann@student.unimelb.edu.au*

Abstract: The interaction of a focused beam with a metasurface supporting dark modes is investigated. We show computationally and experimentally that the excitation of dark modes is accompanied by characteristic changes in the reflected Fourier spectrum. This spatial frequency filtering capability indicates an avenue for the all-optical, on-chip detection of phase gradients for biological and other imaging techniques.

© 2018 Optical Society of America under the terms of the OSA Open Access Publishing Agreement

1. Introduction

Subradiant or 'dark' modes of nanophotonic elements have attracted considerable interest as a result of their long radiative lifetime and associated narrow spectral features [1–9]. These modes possess zero net dipole moment and have symmetries precluding their coupling to a normal plane wave. Examples include the Transverse Electromagnetic (TEM) mode of coaxial cavities [10,11], magnetic dipole modes of split ring resonators [12], and modes of ensembles of nanoparticles exhibiting a radial symmetry [1,2,13]. Their spectral properties can be observed through excitation with off-normal incidence plane waves [8], or vector beams [2,4,13]. Applications of metasurfaces [14,15], consisting of arrangements of nanophotonic resonators on a two-dimensional surface have also progressed with recent demonstrations of their performance as compact lenses [16–18], holograms [19,20], and waveplates [21–24].

Although most research has focused on the utilization of bright modes, the angular sensitivity of the excitation of subradiant modes implies spatial frequency filtering capabilities. This suggests their potential use as ultra-compact alternatives to analogue optical information processing techniques with applications in biological imaging and high precision thickness measurements. Recent publications in this realm have demonstrated advances towards ultra-compact solutions for phase sensing [25], and image processing [26,27], based on plasmonic effects. These theoretically and/or experimentally demonstrate the application of spatial frequency filtering to performing mathematical operations including edge enhancement and the visualization of phase objects.

Here we report on illumination of metasurfaces through high numerical aperture (NA) microscope objectives. The angular spectrum components of the incident field corresponding to off-normal illumination with appropriate polarization can excite subradiant modes of the unit cells, which, here, consist of a radial trimer of silver nanorods. It has previously been shown [2] that as the separation between the rods decreases, the dipole resonance associated with uncoupled particles splits/hybridizes and the dipole mode of the ensemble is red-shifted while the dark mode is blue shifted. This increases the spectral separation between these resonances facilitating identification of each mode. The excitation of dark modes in isolated rod trimer structures and the role played by asymmetries in the geometry has been investigated experimentally [2]. Rather than considering isolated resonators, here we consider

#335803 https://doi.org/10.1364/OSAC.1.000727
Journal © 2018 Received 26 Jun 2018; revised 11 Sep 2018; accepted 20 Sep 2018; published 11 Oct 2018

OSA CONTINUUM

a metasurface consisting of an array of trimer structures (Fig. 1) illuminated through a microscope objective thus taking into account effects due to diffraction and inter cell coupling not present in isolated structures. This provides a broad spectrum of incident spatial frequencies and we show that features in the reflectance spectra, identifiable with dark modes, are apparent and that when the metasurfaces are illuminated with a narrow band of wavelengths associated with subradiant mode excitation, the resulting Fourier plane images exhibit a complex angular-spectrum distribution.

2. Results and discussion

The specific metasurface under consideration here is a uniform, two-dimensional square array where the unit cell consists of three, nominally identical, silver nanorods arranged in a symmetric trimer. The period of the array is denoted d, the lengths of the rods are taken to be ℓ, their widths w and height h. The distance between the center of each rod and the centroid of the arrangement is taken to be s. A schematic is shown in the inset in Fig. 1.

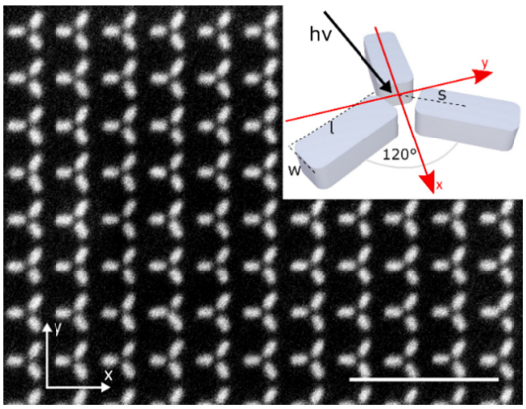

Fig. 1. Array of radial trimers. Scanning electron microscope (SEM) image of the device under investigation with the inset defining parameters used. Scale bar is 1 μm.

To fabricate the metasurface, structure patterns were written into a bilayer of polymethyl methacrylate (PMMA: 80 nm A2 on top of 200 nm LMA EL6, baked at 180°C for 3min after each deposition) resist spun onto a microscope glass slide, using electron beam lithography (Vistec EBPG 5000) and the sample developed in a 3:1 mixture of isopropanol: methyl isobutyl. A 40 nm thick film of silver was deposited using physical vapor deposition on a 2 nm adhesion layer of germanium. Lift-off was performed in acetone. The sample was then immediately encapsulated under a 1 μm-thick PMMA layer so that the resulting metallic nanostructures were embedded in a nearly homogeneous environment for the silver structures to be protected from degradation resulting from exposure to air. A representative SEM image of the fabricated structure is shown in Fig. 1. Analysis of SEM images of this structure indicates that the length of the rods is 104 ± 7 nm, their width is 61 ± 4 nm and the distance between the center of each rod and the centroid of the configuration is 75 ± 5 nm. The periodicity is 304 ± 9 nm.

Figure 2 shows a plot of the reflectance as a function of incident free-space wavelength λ from this array calculated using the Finite Element Method (FEM) as implemented in COMSOL Multiphysics 5.3 with RF module. The optical constants of silver were taken from reference [30]. The dimensions used in the simulation were those obtained from the SEM given above. The array is assumed to be embedded in a homogeneous environment of refractive index 1.5. Periodic boundary conditions were used on the transverse boundaries and ports on the excitation and exit surfaces. The reflectance normalized to the incident power is obtained from the S-parameter S11 and plotted in Fig. 2 for different polarizations and angles of incidence. Figure 2(a) and 2(b) show the reflectance for a normally incident, linearly

OSA CONTINUUM

polarized plane wave when the incident polarization is in the x- (a) and y- (b) directions. A strong dipole resonance near 710 nm (for x-polarization) and 740 nm (for y-polarization), as evidenced by the insets showing the surface charge density at the indicated wavelengths, is apparent. The polarization sensitivity arises from differences in coupling between the unit cells in both x- and y-directions.

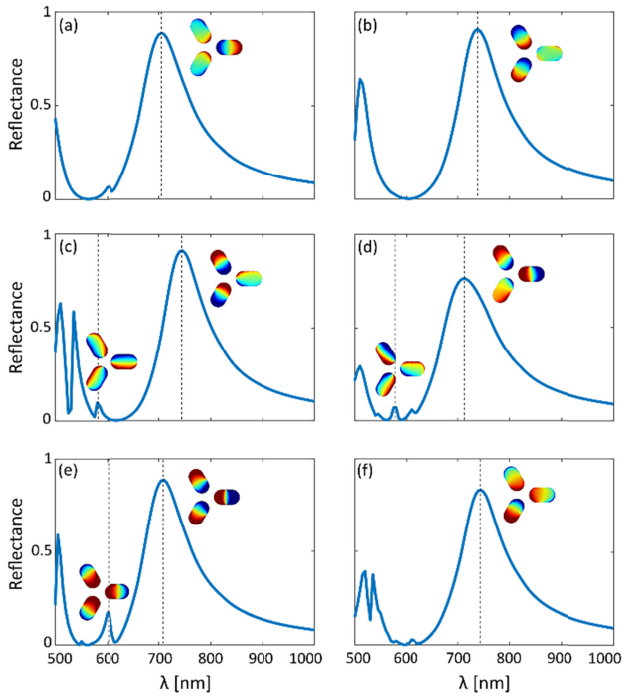

Fig. 2. Calculated normalized reflectance from the metasurface when illuminated with a linearly polarized plane wave. Normal incidence (a, b) for x- (a) and y- (b) polarized and for s- (c, d) and p- (e, f) polarization at 12.5° angle of incidence with the transverse component of the transverse component of the incident wavevector along the x- (c, e) and y- (d, f) directions.

Figure 2(c) and 2(d) show how the spectrum of light reflected from the arrays of trimers is modified when the light is incident at an angle of 12.5°, for cases of s- (TE) polarisation with the transverse component of the electric field aligned in the x- (c) and y- (d) axes of the arrays. In both cases new resonances near 580 nm appear. These resonances were not present under normal incidence indicating their zero net dipolar moment. The surface charge densities on the metallic particles support this identification indicating that these are the result of the excitation of a mode with azimuthal symmetry and near-zero net electric dipole moment – a dark mode. Figures 2(e) and 2(f) show the equivalent results for incident p-(TM) polarized illumination. In this case a different dark mode with a radial symmetry appears near a wavelength of 600 nm for incident illumination parallel to the x-z plane. This mode is only weakly excited for illumination in the y-z plane at a longer wavelength of approximately 610 nm. It is apparent from Fig. 1 that the gap between the elements of different unit cells is less along the y-direction than the x-direction. The illumination producing Fig. 2(f) is polarized along the y-direction and coupling between unit cells could be expected to be relatively strong producing suppression of the dark mode in this case due to the proximity of the nanorods and the symmetry of the charge distribution for this mode.

Given the sensitivity to angle of incidence and polarization at wavelengths associated with dark mode excitation apparent in Fig. 2, we expect characteristic structures to appear in a Fourier plane image at these wavelengths. In particular, the excitation of a dark mode should

OSA CONTINUUM

have a Fourier plane image with low spatial frequencies suppressed, whereas bright mode excitation would have a more uniform Fourier image.

In Fig. 3 we show calculated Fourier-plane images of the light reflected from the trimer array for (a,b) 580 nm, (c,d) 600 nm and (e,f) 740 nm for s (a,c,e) and p (b,d,f) polarization. The suppressed reflectance of low spatial frequencies (located in the center of each image) at 580 nm and 600 nm is a result of the excitation of dark modes that do not couple to normally incident plane waves.

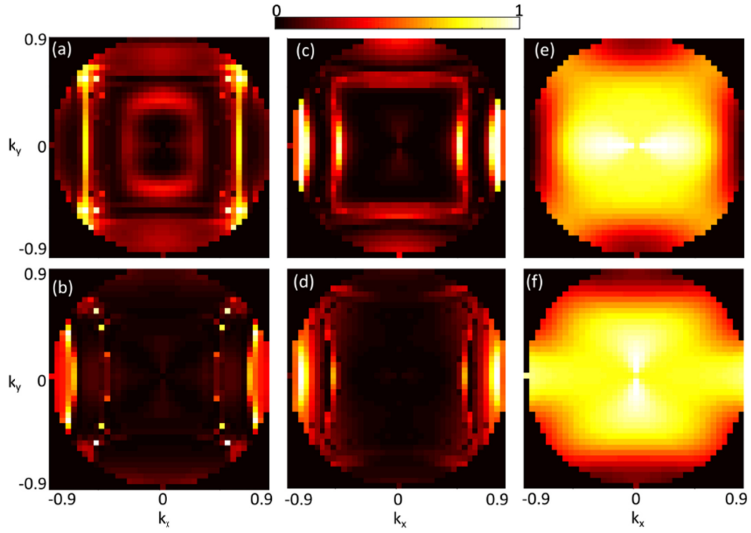

Fig. 3. Computed reflectivities of the metasurface for (a,c,e) s-, and (b,d,f) p-polarized incident illumination at wavelengths of 580 nm (a, b), 600 nm (c, d) and 740 nm (e, f).

At 600 nm, we see the excitation of a mode where the dipole moments excited on the nanorods are radially oriented. This mode, however, is suppressed for an incident wavevector along the y-z-direction. In the case of s-polarization, however, the dark magnetic mode excitation at 580 nm is independent of the direction of the incident wavevector. At 740 nm, on the other hand, there is strong reflectance at normal incidence. The complex spatial-frequency dependence is associated with the fact that the trimers are in an array with significant coupling between unit cells that depends on the direction of incidence. It should be noted that reflection enhancement due to diffraction effects occurs at higher angles in (a-d). However, due to the sharp spatial signature of these, their presence alone cannot explain the demonstrated Fourier plane images.

Here we are specifically interested in the response of the surface to linearly polarized light, we compute the expected Fourier plane images for linearly polarized light incident on a lens from the results for s- and p- polarized light. Using the results of references [31, 32], the Fourier plane intensity when the objective is illuminated with x-polarized light takes the form

$$I_x(k_x,k_y)=\frac{k_x^2R_p(k_x,k_y)+k_y^2R_s(k_x,k_y)}{k_x^2+k_y^2} \qquad (1)$$

where k_x (k_y) is the spatial frequency (normalized to the wavenumber $k_0=2\pi/\lambda$) in the x(y)-direction and R_p (R_s) is the reflectance of p- (s-) polarized light. Equation (1) ignores any contribution from the cross-polarized component which in this case is negligible.

Using the results provided with Fig. 3, Eq. (1) was used to calculate the corresponding Fourier plane images for x-polarized light (Fig. 4). In the following we limit our considerations to x-polarized light due to the clear signature of sub- and super radiant mode in the reflectance spectra. In the case of y-polarized light strong inter-cell coupling occurs,

OSA CONTINUUM

causing additional mode splitting and thereby introducing additional degrees of complexity not resolvable with our current setup.

Again, for x- polarized light a complex Fourier plane image would be anticipated based on the simulations obtained in Fig. 3. for p- and s- polarization. Here we obtain the Fourier plane image for the dark mode under x- polarized illumination [Fig. 4(a)] by averaging both contributions at 580 and 600 nm. This is a valid approach since we can assume significant experimental overlap between both subradiant modes supported by the metasurface due to broadening of the resonances compared to those found in simulations. The result for x-polarized light in Fig. 4(a) again shows a suppression of reflectance at low spatial frequencies as expected for dark mode excitation. At 740 nm [Fig. 4(b)], we see that excitation of the bright mode produces stronger reflection at low spatial frequencies in line with expectations.

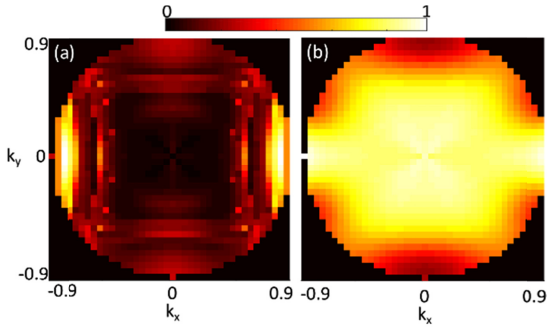

Fig. 4. Computed averaged reflectivities of the metasurface for x-polarized incident illumination at the (a) dark- and (b) bright mode wavelengths.

The measurement of reflectance from the fabricated metasurface was performed using the benchtop optical set up shown in Fig. 5.

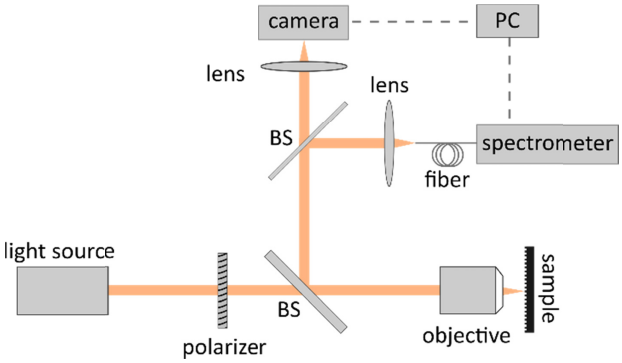

Fig. 5. Experimental set-up for the measurement of reflectance spectra and Fourier plane images.

Collimated, linearly polarized light from a tungsten-halogen bulb (Ocean Optics HL-2000) was transmitted through an infinity corrected NA 0.90 Nikon Plan NCG x100 objective to illuminate the sample. Although the light incident on the objective was linearly polarized in either the x- or y-direction, it is noted that the illumination onto the sample will consist of a superposition of s- and p- polarized light introducing a complex incident angular spectrum.

The reflected light was sent via a beam splitter (Thorlabs CM1-BS013) and a thin film beam splitter (Thorlabs BSW013) to a spectrometer (Ocean Optics QE65000). The spectra obtained were normalized to those obtained from an unpatterned region of the sample. The results are shown in Fig. 6. For both polarizations, spectra are dominated by a broad peak at a wavelength just longer than 700 nm. Another broad peak near 520 nm is also apparent. We

OSA CONTINUUM

can assign this to a dipole mode along the short axis of the rods as well as lattice diffraction based on numerical calculations. A weaker feature around 630 nm is also apparent.

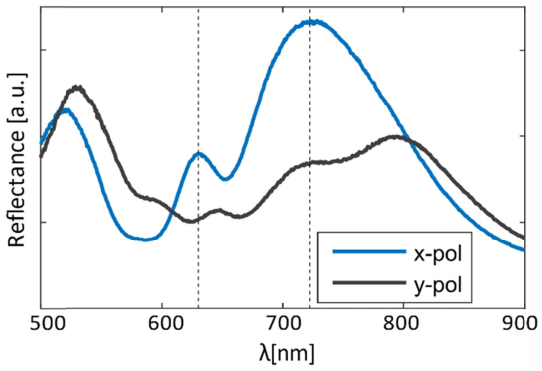

Fig. 6. Experimentally obtained reflectance spectra from the device of Fig. 1 when illuminated through an objective with an NA 0.9.

We hypothesize that this corresponds to excitation of one or both of the two dark modes identified in the simulations of Fig. 2. To test this assertion, we obtain Fourier plane images of the reflection from the sample using the set-up shown in Fig. 5 with the spectrometer beam splitter removed. An image of the back focal plane of the objective is obtained on a CMOS camera using a f = 50.0 mm lens (Thorlabs LA1131-A) and illuminating the sample using the NA 0.9 objective. The original source is replaced with a supercontinuum laser source (Fianium SC-450-2) which is passed through a fiber-coupled tunable filter (Fianium Superchrome VIS-FDS-MM) set to its minimum bandwidth of 10 nm. Fourier plane images were obtained with the central wavelength incident illumination set to values ranging from 549 nm to 741 nm covering the features indicated in the spectra of Fig. 6. The results are shown in Fig. 7.

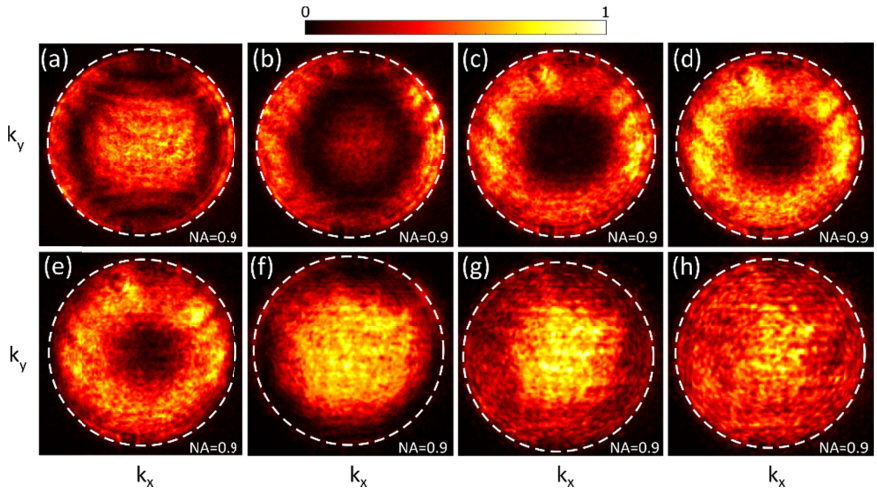

Fig. 7. Normalized Fourier plane images obtained using x-polarized light with central wavelengths 549 nm (a), 578 nm (b), 616 nm (c), 626 nm (d), 635 nm (e), 674 nm (f), 714 nm (g), 741 nm (h) and a bandwidth of approximately 10 nm.

Considering Fig. 7(c) and 7(d), obtained at 616 and 626 nm where we expect dark mode excitation, we observe that the suppressed reflectance at low spatial frequencies agrees with the expected Fourier characteristics for subradiant modes derived in Fig. 4. The residual

OSA CONTINUUM

reflectance in this regime is a result of contributions from the strong bright mode and background reflections from the interface between the glass and air. From 674 nm upwards [Fig. 7(f)–7(h)], however, a more uniform intensity that gradually decreases with increasing spatial frequency can be observed providing reasonable agreement with the expected Fourier characteristic of a radiant mode [Fig. 4(b)]. A similar pattern is apparent in the green region of the spectrum [Fig. 7(a) and 7(b)] where we expect excitation of a dipole mode with dipole moment parallel to the short axis of the nanorods. Additionally, characteristic diffraction lines are apparent at these wavelengths in line with expectations. The spatial frequency filtering capability of the metasurface is apparent in in Fig. 8 where line profiles through the vertical and horizontal center of Fig. 7(d) and 7(g) are shown.

We clearly have been able to experimentally distinguish between the excitation of the dipole mode and the subradiant modes in the reflection spectrum (Fig. 6) as well as the Fourier plane images (Fig. 7). Due to the imperfections of the fabricated metasurface, the near-degeneracy of the two dark modes (spectral separation of approximately 20 nm) and the illumination bandwidth, the data of Fig. 7 cannot distinguish the excitation of the two relevant subradiant modes for which a direct comparison between simulation and experimental results is omitted here.

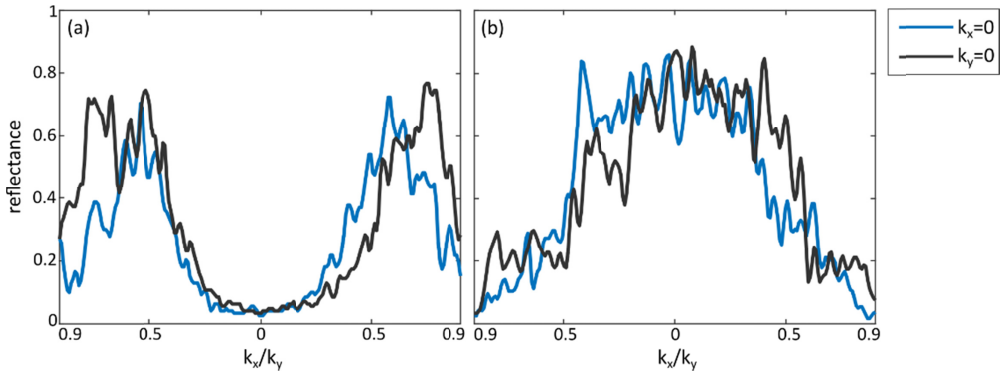

Fig. 8. Line profiles along $k_x = 0$ and $k_y = 0$ of Fourier plane images [Fig. 7(d) and 7(g)] at (a) 626 nm and (b) 714 nm illustrating quantitative spatial frequency filtering.

3. Conclusion

In conclusion, we have probed the presence of subradiant modes of unit cells of a plasmonic metasurface using high NA (0.9) illumination. This permits access to a wide range of incident spatial frequencies with Fourier plane imaging indicating a complex spatial frequency sensitivity for subradiant modes. Experimental results support the broad conclusions of simulated results, but more precise experiments should be able to elucidate more information about the angular spectrum sensitivity of metasurfaces supporting dark modes. The structure presented here supports two different dark modes presenting the intriguing possibility of being further able to tune the resonant properties of these metasurfaces. Furthermore, coupling between unit cells influences the angular spectrum of reflected light introducing additional degrees of freedom. Potential applications of this research lie in the broad area of optical information processing where the utilization of subradiant modes of nanostructures permits the creation of metasurfaces sensitive to the angular spectrum of transmitted or reflected optical fields. This capability provides an avenue for the development of ultracompact devices that can perform on-chip, real-time, single-shot conversion of phase information to readily measured intensity distributions for live-cell microscopy and imaging of other transparent objects.

OSA CONTINUUM

Funding

Australian Research Council Discovery Projects (DP160100983) and Future Fellowship scheme (FT140100514).

Acknowledgments

This work was performed in part at the Melbourne Centre for Nanofabrication (MCN) in the Victorian Node of the Australian National Fabrication Facility (ANFF).

References

1. Z.-L. Deng, T. Fu, Z. Ouyang, and G. P. Wang, "Trimeric metasurfaces for independent control of bright and dark modes of Fano resonances," Appl. Phys. Lett. **108**(8), 081109 (2016).
2. D. E. Gómez, Z. Q. Teo, M. Altissimo, T. J. Davis, S. Earl, and A. Roberts, "The dark side of plasmonics," Nano Lett. **13**(8), 3722–3728 (2013).
3. B. Gallinet and O. J. Martin, "Refractive index sensing with subradiant modes: a framework to reduce losses in plasmonic nanostructures," ACS Nano **7**(8), 6978–6987 (2013).
4. J. Sancho-Parramon and S. Bosch, "Dark modes and Fano resonances in plasmonic clusters excited by cylindrical vector beams," ACS Nano **6**(9), 8415–8423 (2012).
5. Y.-C. Chang, S.-M. Wang, H.-C. Chung, C.-B. Tseng, and S.-H. Chang, "Observation of absorption-dominated bonding dark plasmon mode from metal-insulator-metal nanodisk arrays fabricated by nanospherical-lens lithography," ACS Nano **6**(4), 3390–3396 (2012).
6. B. Luk'yanchuk, N. I. Zheludev, S. A. Maier, N. J. Halas, P. Nordlander, H. Giessen, and C. T. Chong, "The Fano resonance in plasmonic nanostructures and metamaterials," Nat. Mater. **9**(9), 707–715 (2010).
7. M. Liu, T.-W. Lee, S. K. Gray, P. Guyot-Sionnest, and M. Pelton, "Excitation of dark plasmons in metal nanoparticles by a localized emitter," Phys. Rev. Lett. **102**(10), 107401 (2009).
8. F. Hao, E. M. Larsson, T. A. Ali, D. S. Sutherland, and P. Nordlander, "Shedding light on dark plasmons in gold nanorings," Chem. Phys. Lett. **458**(4-6), 262–266 (2008).
9. M.-W. Chu, V. Myroshnychenko, C. H. Chen, J.-P. Deng, C.-Y. Mou, and F. J. García de Abajo, "Probing bright and dark surface-plasmon modes in individual and coupled noble metal nanoparticles using an electron beam," Nano Lett. **9**(1), 399–404 (2009).
10. F. I. Baida, "Enhanced transmission through subwavelength metallic coaxial apertures by excitation of the TEM mode," Appl. Phys. B **89**(2-3), 145–149 (2007).
11. A. Roberts and R. C. McPhedran, "Bandpass grids with annular apertures," IEEE Trans. Antenn. Propag. **36**(5), 607–611 (1988).
12. S. Mühlig, C. Menzel, C. Rockstuhl, and F. Lederer, "Multipole analysis of meta-atoms," Metamaterials (Amst.) **5**(2-3), 64–73 (2011).
13. A. Yanai, M. Grajower, G. M. Lerman, M. Hentschel, H. Giessen, and U. Levy, "Near- and far-field properties of plasmonic oligomers under radially and azimuthally polarized light excitation," ACS Nano **8**(5), 4969–4974 (2014).
14. N. Yu and F. Capasso, "Flat optics with designer metasurfaces," Nat. Mater. **13**(2), 139–150 (2014).
15. A. V. Kildishev, A. Boltasseva, and V. M. Shalaev, "Planar photonics with metasurfaces," Science **339**(6125), 1232009 (2013).
16. A. Pors, M. G. Nielsen, R. L. Eriksen, and S. I. Bozhevolnyi, "Broadband focusing flat mirrors based on plasmonic gradient metasurfaces," Nano Lett. **13**(2), 829–834 (2013).
17. L. Lin, X. M. Goh, L. P. McGuinness, and A. Roberts, "Plasmonic lenses formed by two-dimensional nanometric cross-shaped aperture arrays for Fresnel-region focusing," Nano Lett. **10**(5), 1936–1940 (2010).
18. X. M. Goh, L. Lin, and A. Roberts, "Planar focusing elements using spatially varying near-resonant aperture arrays," Opt. Express **18**(11), 11683–11688 (2010).
19. G. Zheng, H. Mühlenbernd, M. Kenney, G. Li, T. Zentgraf, and S. Zhang, "Metasurface holograms reaching 80% efficiency," Nat. Nanotechnol. **10**(4), 308–312 (2015).
20. P. Genevet and F. Capasso, "Holographic optical metasurfaces: a review of current progress," Rep. Prog. Phys. **78**(2), 024401 (2015).
21. J. J. Cadusch, T. D. James, and A. Roberts, "Experimental demonstration of a wave plate utilizing localized plasmonic resonances in nanoapertures," Opt. Express **21**(23), 28450–28455 (2013).
22. T. Ellenbogen, K. Seo, and K. B. Crozier, "Chromatic plasmonic polarizers for active visible color filtering and polarimetry," Nano Lett. **12**(2), 1026–1031 (2012).
23. J. Yang and J. Zhang, "Subwavelength quarter-waveplate composed of L-shaped metal nanoparticles," Plasmonics **6**(2), 251–254 (2011).
24. E. H. Khoo, E. P. Li, and K. B. Crozier, "Plasmonic wave plate based on subwavelength nanoslits," Opt. Lett. **36**(13), 2498–2500 (2011).
25. F. Eftekhari, D. E. Gómez, and T. J. Davis, "Measuring subwavelength phase differences with a plasmonic circuit-an example of nanoscale optical signal processing," Opt. Lett. **39**(10), 2994–2997 (2014).

OSA CONTINUUM

26. T. Zhu, Y. Zhou, Y. Lou, H. Ye, M. Qiu, Z. Ruan, and S. Fan, "Plasmonic computing of spatial differentiation," Nat. Commun. **8**, 15391 (2017).
27. A. Silva, F. Monticone, G. Castaldi, V. Galdi, A. Alù, and N. Engheta, "Performing mathematical operations with metamaterials," Science **343**(6167), 160–163 (2014).

128.250.28.203 {ts '2020-10-12 00:58:23'}